EasyChair Preprint

№ 4772

Numerical study on flow, heat transfer and entropy generation of supercritical co2 in a heated helical coiled tube

Mohammed Baghdad and Ahmed Ouadha

December 23, 2020

NUMERICAL STUDY ON FLOW, HEAT TRANSFER AND ENTROPY GENERATION OF SUPERCRITICAL CO_2 IN A HEATED HELICAL COILED TUBE

M. Baghdad[1,2*], A.Ouadha[1]
[1]Laboratoire des Sciences et Ingénierie Maritimes, Faculté de Génie Mécanique,
Université des Sciences et de la Technologie Mohamed Boudiaf d'Oran, Oran El-Mnouar, 31000 Oran, Algeria
[2]Institut des Sciences et Technologie, Centre Universitaire de Tissemsilt,
B.P. 182, 38000 Tissemsilt, Algeria.
*Corresponding author: E-mail: baghdad.cut@gmail.com

ABSTRACT
The present paper aims to numerically investigate the flow, heat transfer and entropy generation of sCO_2 in a heated helical coiled tube having an inner diameter of 9.0 mm, a length of 5500 mm and 6 turns of coils with a pitch distance of 32 mm. Computations have been carried out using SST k-ω turbulence model and considering sCO_2 as a real gas. Two inlet boundary conditions, mass flow rate inlet and pressure inlet, have been tested with various wall heat flux values. Results, in terms of pressure drop and Nusselt number, showed good agreement with experimental measurements from the literature. Furthermore, results obtained provide detailed flow, heat transfer and irreversibilities information for further design and optimization of sCO_2equipments for industrial applications.

Keywords: *heat transfer, entropy generation, supercritical CO_2, helical tube*

1. INTRODUCTION
Heat transfer is present in all energy utilization systems. The enhancement of heat transfer performance will significantly contribute to the energy conservation in energy systems. Heat exchangers composed of helically coiled tubes present the advantage of compactness and enhanced heat transfer.
Supercritical carbon dioxide (sCO_2) helically coiled gas heaters have received particular interest during the last years due to their compact structure and the preeminent thermal and flow properties of sCO_2. Thermophysical properties of sCO_2 such as the specific heat capacity, density, viscosity and thermal conductivity undergo significant variations. The flow and heat transfer characteristics are related to these thermophysical properties and operating and tubes geometrical parameters.
Several experimental and numerical studies on the flow characteristics of sCO_2 in helical coiled tubes with different geometries (tube diameter, diameter and pitch of the coil) have been carried out by many researchers [Wang et al., 2013 ; Xu et al., 2015 ; Xu et al., 2018 ; Li et al., 2018 ; Bai et al., 2019 ; Liu et al., 2019]. The inlet pressure has been varied from 7.5 to 23 MPa with a mass flux from 0 to 1100 $kg/m^2.s$, and a heat flux imposed on the wall ranging from 0 to 300 kW/m^2. The results indicate that heat and mass fluxes have significant effects on the flow characteristics of the fluid.
Liu et al. (2018) have shown experimentally that the heat transfer coefficient tripled when the diameter of the tube passes from 4 to 2 mm and it increases up to 30% when the diameter of the coil drops from 140 to 36 mm. Zhang et al. (2019) demonstrated that the helical configuration of a tube improves the average heat transfer performance compared to a horizontal tube.
The combined effects of the centrifugal force and buoyancy force on the heat transfer has attracted more attention in the literature through various experimental and numerical studies [Xu et al., 2015 ; Li et al., 2016 ; Zhao et al., 2016 ; Wang et al., 2017 ; Liu et al., 2017 ; Zhang et al., 2018 ;Bai et al., 2018 ; Zhang et al., 2019 (1)]. It is shown that the two forces induce a secondary flow in the cross section which improves the heat transfer characteristics.
The design of efficient thermodynamic processes conserves the useful energy. Fluid flow and heat transfer processes are inherently irreversible. The irreversibilities are mainly due to the entropy generation and thus, destruction of useful energy (exergy). Although that energy is conserved, according to the first law, the quality of the energy is

decreased because energy is converted into a different form of energy. Thus, reducing entropy generated in a process will result in a more efficient design of energy the system.

Since its establishment by Bejan (1982), entropy generation analysis has received a growing interest in optimization of thermal processes. Entropy generation is directly related to thermodynamic irreversibilities, which characterize any real process. Hence, methods based on entropy generation minimization can be considered as a robust tool in the optimization of thermal processes. Although that there have been various areas and subjects where entropy generation calculations have been conducted (Safer et al., 2017), to the best of the authors' knowledge, entropy generation in turbulent flow of sCO_2 in helical coiled tubes has not been studied extensively in the literature. Thus, the objective of the present study is to numerically investigate the the flow, heat transfer and entropy generation of sCO_2 in a heated helically coiled tube. Computations have been carried out using *SST k-ω* turbulence model and considering sCO_2 as a real gas.

2. MATHEMATICAL MODELING AND SIMULATION METHOD

2.1 Physical domain

Figure 1 shows a schematic representation of the configuration of the helically tube studied. It is described by the diameter of the tube (d = 9 mm), the diameter of the coil (D = 283 mm) and the pitch of the coil (p = 32 mm); with 6 turns in the coil of total length of the tube 5500 mm. The tube is positioned vertically so that the flow is directed upward, against the direction of gravity. This configuration has been the subject of an experimental study by Wang et al. (2015), Zhang et al. (2015) and Xu et al. (2015). This case has been also numerically studied by Zhang et al. (2018) and Bay et al. (2018).

2.2 Governing equations and boundary layers

The flow of sCO2 within the helically coiled tube is considered steady, compressible and 3D. Equations composed the CFD model used are briefly described in this section. The CFD model solves the steady Favre averaged Navier-Stoke equations:

$$\frac{\partial}{\partial x_i}\left(\rho u_i\right)=0 \tag{1}$$

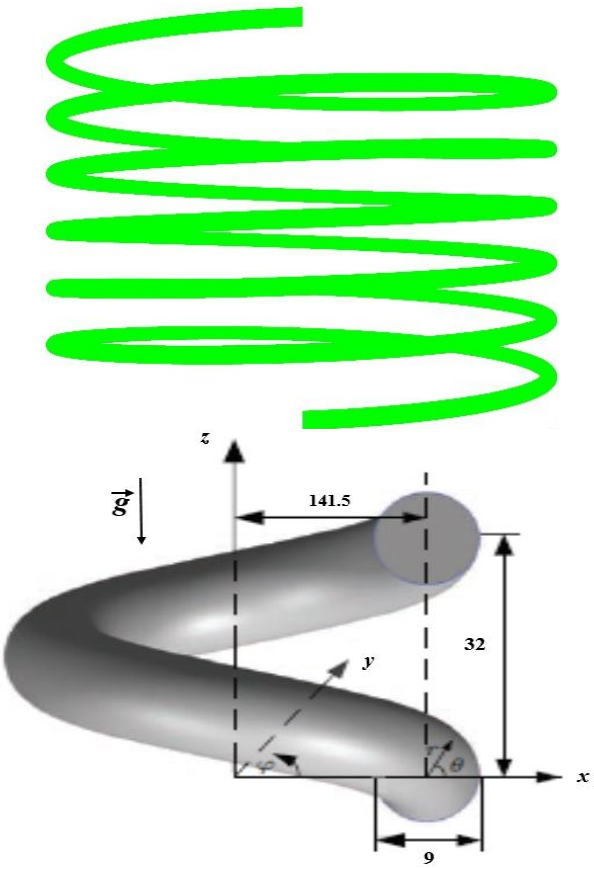

Figure 1. Physical domain : *a*. General view 3D ; *b*. Dimensions (in mm) with coordinate system

$$\frac{\partial}{\partial x_i}\left(\rho u_i u_j\right)=\rho g_i-\frac{\partial p}{\partial x_i}+\frac{\partial}{\partial x_j}\left[\left(\mu+\mu_t\right)\frac{\partial u_i}{\partial x_j}\right] \tag{2}$$

$$\frac{\partial}{\partial x_i}\left(u_i\left(\rho E+p\right)\right)=\frac{\partial}{\partial x_i}\left(\lambda\frac{\partial T}{\partial x_i}+u_i\tau_{ij}\right) \tag{3}$$

where ρ, u_i, p et E denote density, velocity components, static pressure and the total volumetric energy. μ_t is the turbulent viscosity and τ_{ij} is the Reynolds stresses:

$$\mu_t=C_\mu\rho\frac{k^2}{\varepsilon}\left(\frac{\partial u_i}{\partial x_j}+\frac{\partial u_j}{\partial x_i}\right)-\frac{2}{3}\mu\frac{\partial u_i}{\partial x_i}\delta_{ij} \tag{4}$$

where C_μ is a constant, ρ is the steam density, and k and ε are two additional independent variables, which need to be modeled and solved in a similar way as velocities.

A turbulence model is needed to model the unknown Reynolds stresses through turbulent eddy viscosity, μ_t. In the present study, the *SST k-ω* turbulence model (Menter, 1994) is used.

A mass flux has been specified at the inlet of the tube, while an outflow condition has been selected at the outlet. For the wall boundaries, a no-slip

condition with a proper wall treatment approach with a y^+ up to 1.2 has been adopted.

The heat transfer coefficient is calculated by the following relationship:

$$h = q_w / (T_w - T_b) \quad (5)$$

where T_w is the average circumferential wall temperature and T_b is the temperature at the cross section which is defined by:

$$T_b = \frac{\int u \rho C_p T \, dA}{\int u \rho C_p \, dA} \quad (6)$$

where *dA* is an elementary area of the cross section of the tube.

2.3 Solution procedure

The mesh has been generated using equidistant hexahedral cells to minimize any errors associated with extrusion, distortion, etc. Figure 2 shows two different views of the generated mesh. The dimensionless thickness of the first grid layer adjacent to the wall for y^+ should be 1 to better describe the gradients near the wall. The values *y+* in the computation mesh are between 0.6 and 1.2.

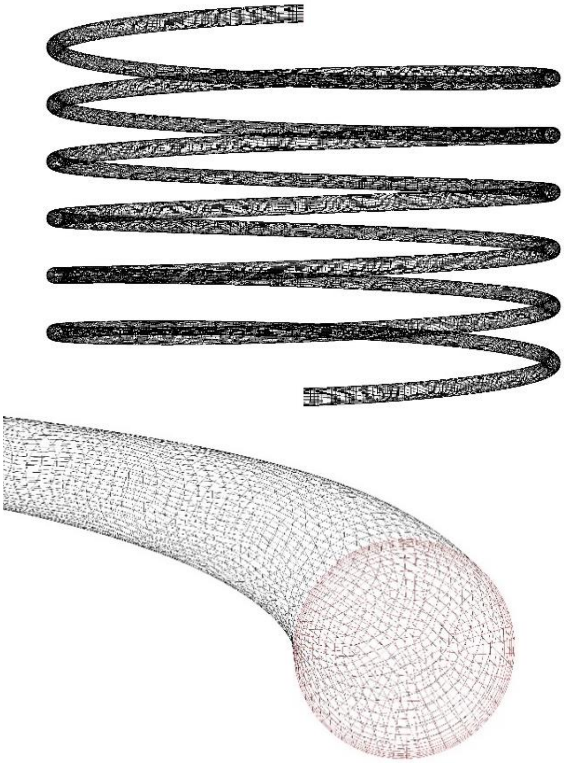

Figure 2. Computational domain and mesh

The CFD model has been built in Ansys Fluent 15.0. A pressure-based solver in steady mode has been used. SIMPLE algorithm has been used for pressure-velocity coupling. QUICK scheme is used for momentum and energy equations, while a second order upwind scheme has been preferred for turbulence equations. Thermophysical properties of sCO2, as a real gas, have been evaluated from the NIST 23 database. Relaxation factors have been adjusted for all variables. Convergence has been assumed reached once the residuals are lower than 10^{-5} for all variables. Besides, the convergence has been further assessed by assuming a mass conservation with an error below 10^{-7}.

The mesh size and quality have a great influence on the calculation results. A mesh study has been first performed before the calculation. Three grids of 1,432,000, 3,363,000 and 5,124,000 cells have been used. Figure 3 shows the variation of the average fluid temperature and the wall temperature along the tube for the three grids. It was observed that the second mesh (3,363,000) provided results similar to those of the third one. It was decided that mesh 2 should be chosen as the mesh for further analysis. Increasing the number of grid cells requires a large computer capacity without a successful simulation guaranty.

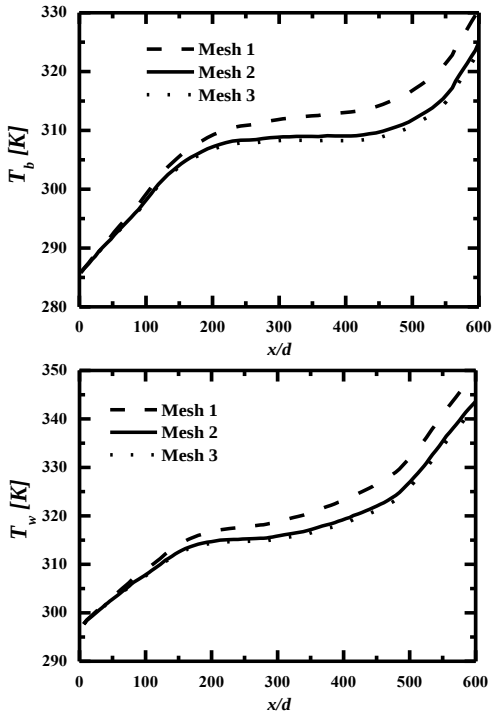

Figure 3. T_b and T_w sensitivity to the mesh size

2.4. Entropy generation

Heat and fluid flow processes are naturally irreversible. The irreversibility originates from entropy generation.

The local rate of entropy generation per unit volume, $\dot{S}_{gen}$, is the sum of entropy generation rate due to viscous dissipation, $S_{gen,v}$, entropy generation rate due to indirect viscous dissipation (turbulence), $S'_{gen,v}$, entropy generation rate due to heat transfer, $S_{gen,T}$ and entropy generation rate due to indirect heat transfer (turbulence), $S'_{gen,T}$, (Kock et Herwig, 2004; Kock et Herwig, 2005):

$$S_{gen} = S_{gen,v} + S'_{gen,v} + S_{gen,T} + S'_{gen,T} \quad (7)$$

The entropy generation components are expressed in Cartesian coordinates, for a 3D flow, as

$$S_{gen,v} = \frac{\mu}{T}\left[\begin{array}{l} 2\left(\left(\frac{\partial u}{\partial x}\right)^2 + \left(\frac{\partial v}{\partial y}\right)^2 + \left(\frac{\partial w}{\partial z}\right)^2\right) \\ + \left(\frac{\partial u}{\partial y} + \frac{\partial v}{\partial x}\right)^2 + \left(\frac{\partial u}{\partial z} + \frac{\partial w}{\partial x}\right)^2 + \left(\frac{\partial v}{\partial z} + \frac{\partial w}{\partial y}\right)^2 \end{array}\right] \quad (8)$$

$$S'_{gen,v} = \frac{\rho\omega}{T} \quad (9)$$

$$S_{gen,T} = \frac{k}{T^2}\left[\left(\frac{\partial^2 T}{\partial x^2}\right)^2 + \left(\frac{\partial^2 T}{\partial y^2}\right)^2 + \left(\frac{\partial^2 T}{\partial z^2}\right)^2\right] \quad (10)$$

$$S'_{gen,T} = \frac{k_t}{T^2}\left[\left(\frac{\partial^2 T}{\partial x^2}\right)^2 + \left(\frac{\partial^2 T}{\partial y^2}\right)^2 + \left(\frac{\partial^2 T}{\partial z^2}\right)^2\right] \quad (11)$$

where ω is the turbulence dissipation rate and k_t is the turbulent thermal conductivity. Their values are defined by the turbulence model used.

To evaluate the relative dominance of entropy generation contributions, Paolleti et al. (1989) introduced a dimensionless parameter called Bejan number (*Be*) and defined as the ratio of heat transfer to total entropy generation:

$$\mathrm{Be} = \frac{S_{gen,T} + S'_{gen,T}}{S_{gen,T} + S'_{gen,T} + S_{gen,v} + S'_{gen,v}} \quad (12)$$

3 RESULTATS ET DISCUSSIONS

3.1 Validation

The computed results are compared with the measurements of Zhang et al. (2015) and Wang et al. (2015) in terms of average fluid and wall temperatures and the heat transfer coefficient. Computations have been performed for an inlet mass flux rate of 97.8 kg/m^2.s and a pressure of 8.02 MPa with a temperature 288 K. The tube wall is subjected to a heat flux of 9.03kW/m^2. Figure 4 illustrates the variation of average fluid temperature, the wall temperature and the coefficient of heat transfer along the tube cross sections. The agreement between the numerical predictions and the experimental results is very good. The discrepancies are less than 1.6% for temperatures and less than 6% for the heat transfer coefficient.

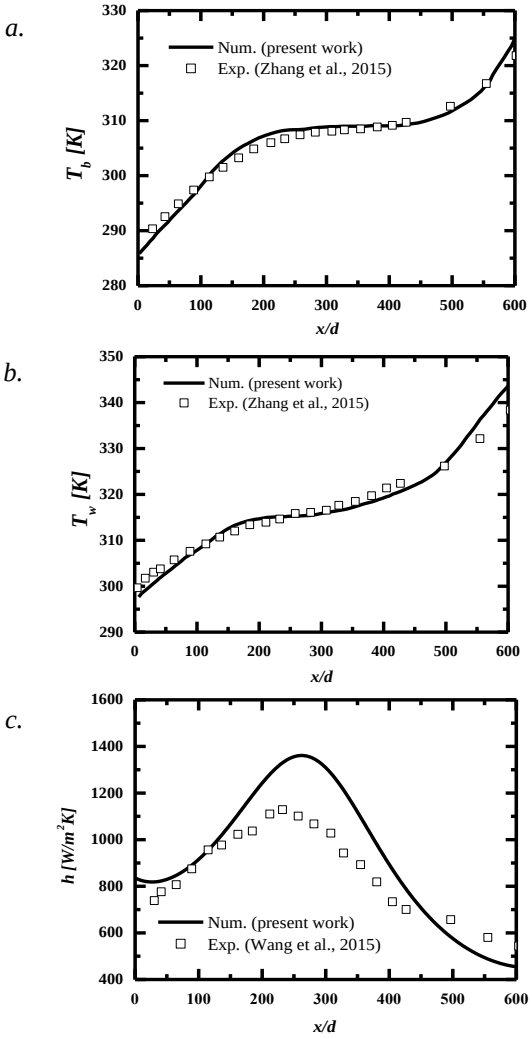

Figure 4. Numerical results versus experimental measurements : *a.* Average fluid temperature ; *b.* Wall temperature ; *c.* Heat transfer coefficient

3.2 Velocity field

The velocity contours are presented in Figure 5 for a mass flux of 97.8 kg/(s.m^2) and a wall heat flux of 9.03 kW/m^2. Contours are displayed from bottom to top along the length of the tube. The selected cross sections are oriented in the same way. The fluid velocity increases from the inlet to the outlet. The acceleration of the fluid causes an increase in the velocity gradient near the wall and distorts the circular shape in the central region of the tube.

3.3 Temperature field

The temperature distribution for the fixed operating conditions (p_{in} = 8.02 MPa, G = 100 kg/m^2.s, q = 9.03 kW/m^2) are shown in Figure 6. A thermal boundary layer was observed near the wall of the tube. It thickens along the tube from inlet to outlet. The temperature contours confirm the velocity results with the increase in fluid temperature in the inner side of the tube. This increase is due to the braking of fluid in this area.

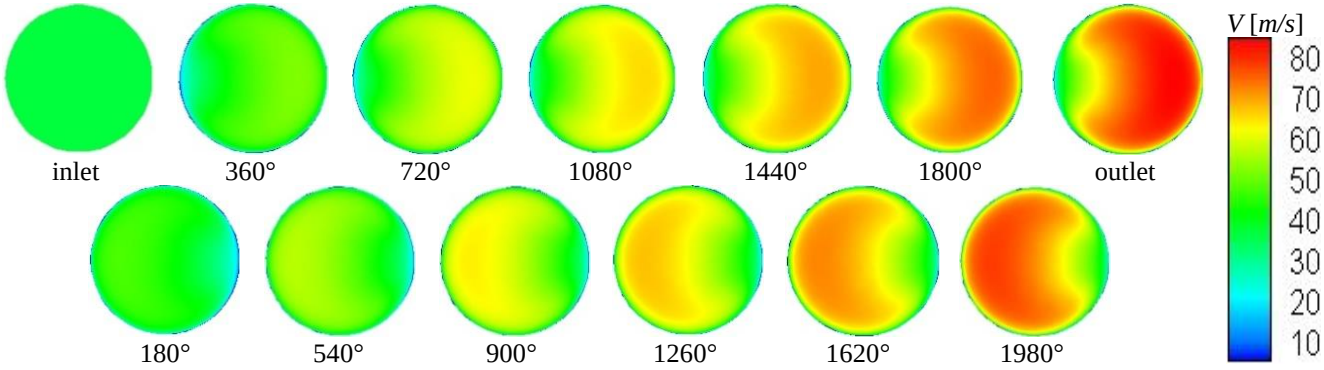

Figure 5. Contours de la vitesse pour différentes sections transversales le long du tube hélicoïdal (P_{in} = 8.02 MPa, G=100 kg/m^2.s, q=9.03 kW/m^2)

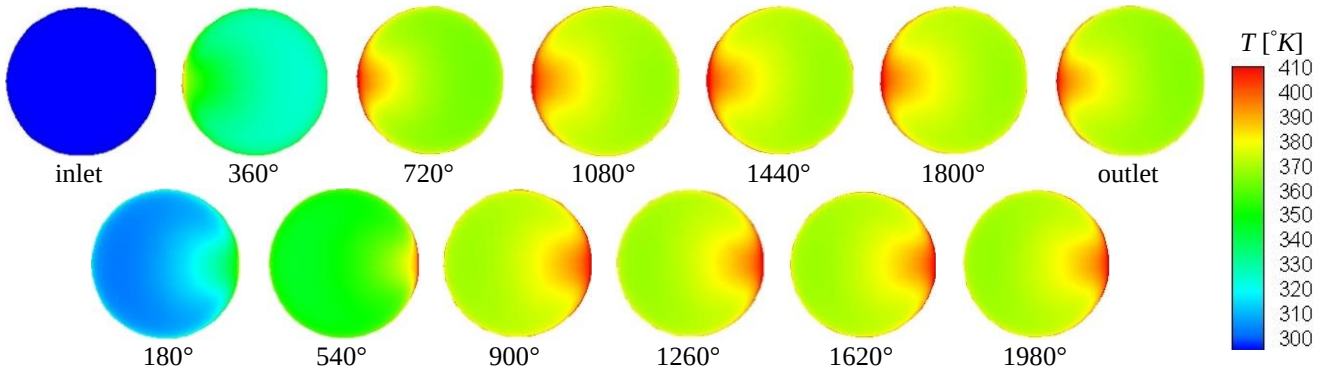

Figure 6. Temperature contours for different cross sections along the tube (p_{in} = 8.02 MPa, G=100 kg/m^2.s, q=9.03 kW/m^2)

The effects of heat fluxes on the heat transfer performance of sco$_2$ in the helically tube are shown in figure 7. As the heat flux increases, the maximum value of the heat transfer coefficient decreases. This can be attributed to the radial

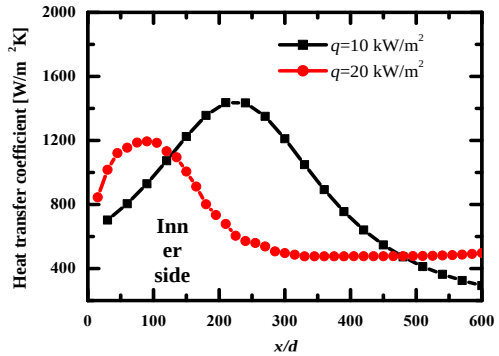

Figure 7. Effect of wall heat flux on the heat transfer coefficient (p_{in} = 8.02 MPa and G=100 kg/m^2.s)

3.4 Entropy generation

3.4.1 Local entropy generation

Figures 8, 9 and 10 show the contours of the local entropy generation rate for different stations in the helically tube. As shown in equations (8) to (11), the entropy generation is mainly calculated by the temperature and velocity gradients. An increase in the temperature gradient indicates an increase in heat transfer performance, while an increase in the velocity gradient implies increased viscous dissipation. The maximum entropy generation values are located in the boundary layer region, since the temperature gradient considerably exceeds that of the main flow region as illustrated in Figure 8. The local entropy generation due to viscous effects is obviously observed in the region of the turbulent pulsation where the fluid has an impact on the tube walls. It is clear that the entropy generation due to viscous effect is lower compared to the

thermal local entropy generation in all the stations of the tube presented (Figure 9). The total entropy generation, sum of the local entropy generation due to viscous effects and the local entropy generation due to heat transfer effect, is shown in Figure 10.

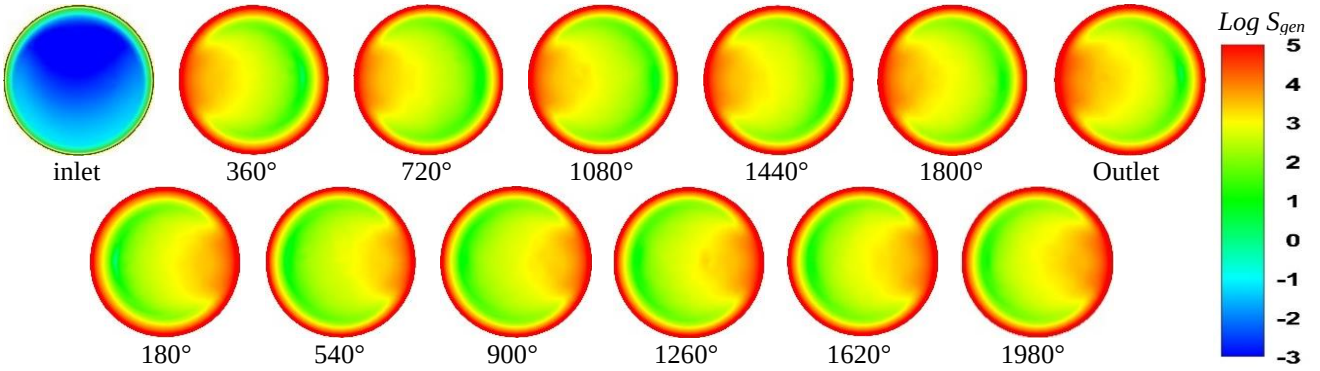

Figure 8. Entropy generation contours due to thermal effects for different cross section along the tube

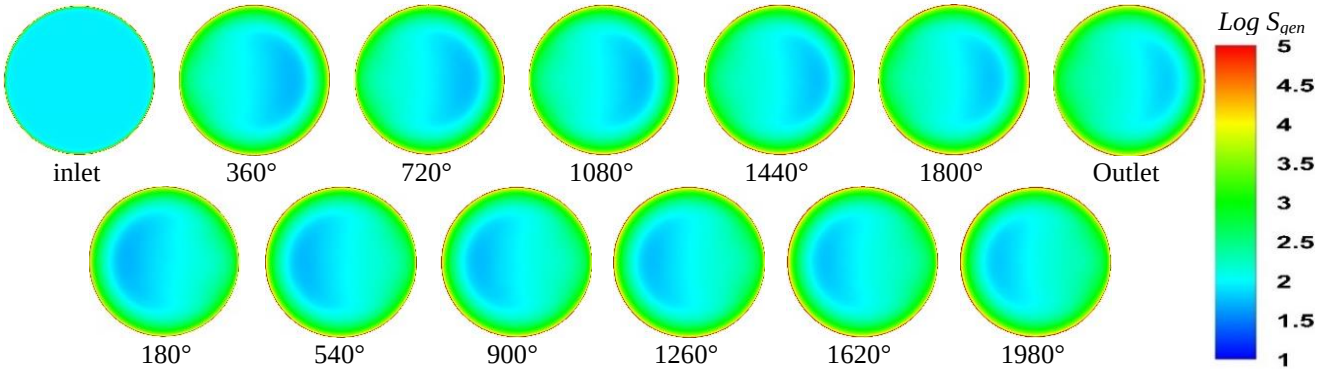

Figure 9. Entropy generation contours due to viscous effects for different cross section along the tube

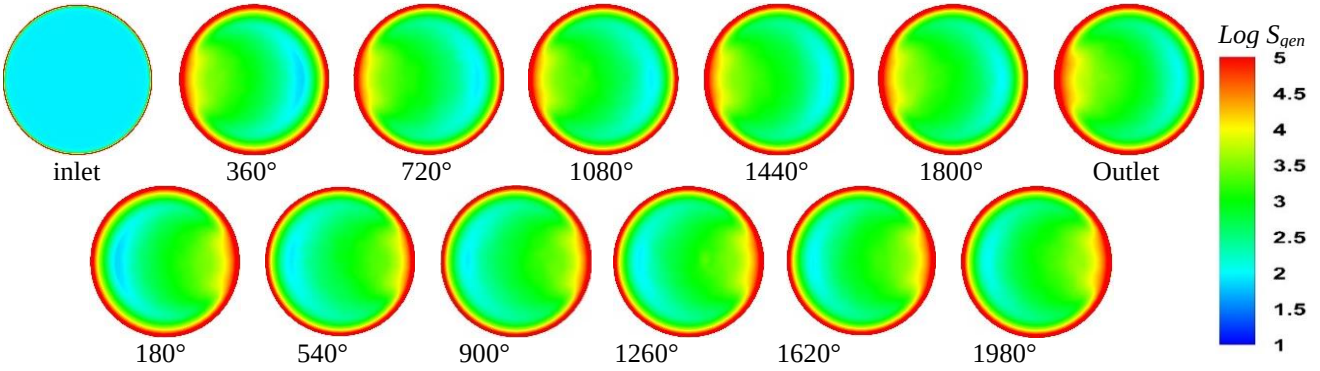

Figure 10. Total entropy generation contours for different cross section along the tube

3.4.2 Average entropy generation

The average entropy generation rates in the tube as a function of the wall heat flux are illustrated in Figure 11. It can be seen that $S_{gen,T}$ increases with the increase in the heat flux, while $S_{gen,v}$ slightly decreases.

3.4.3 Bejan number

The Bejan number is ranged between 0 and 1. The local *Be* is illustrated in Figure 12 to describe the share of the thermal local entropy generation. It is observed that the dominant heat transfer entropy generation region (effective heat transfer zone) is in the layer near walls and a tail-shaped zone. The effective heat transfer zone has a maximum value. The entropy generation due to viscous effect is negligible.

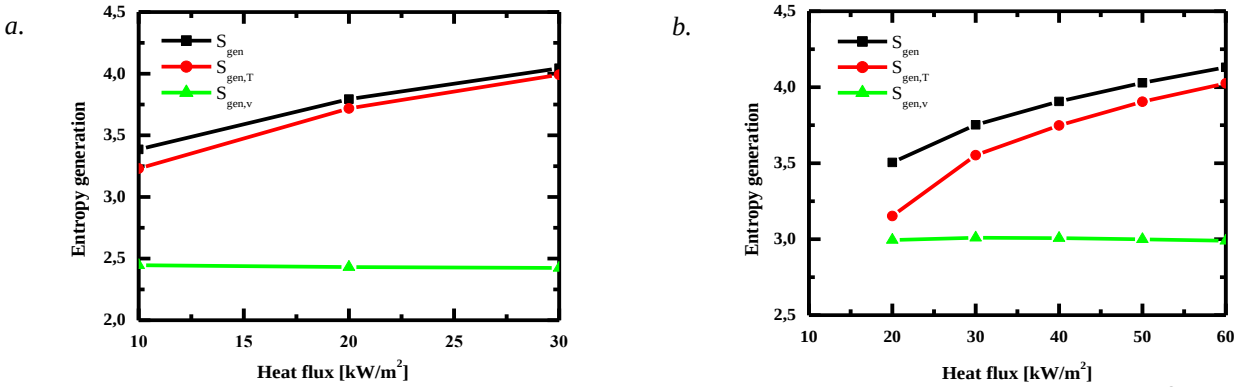

Figure 11. Wall heat flux effect on the entropy generation rate : *a.* G=100, *b.* G=300 kg/m^2.s

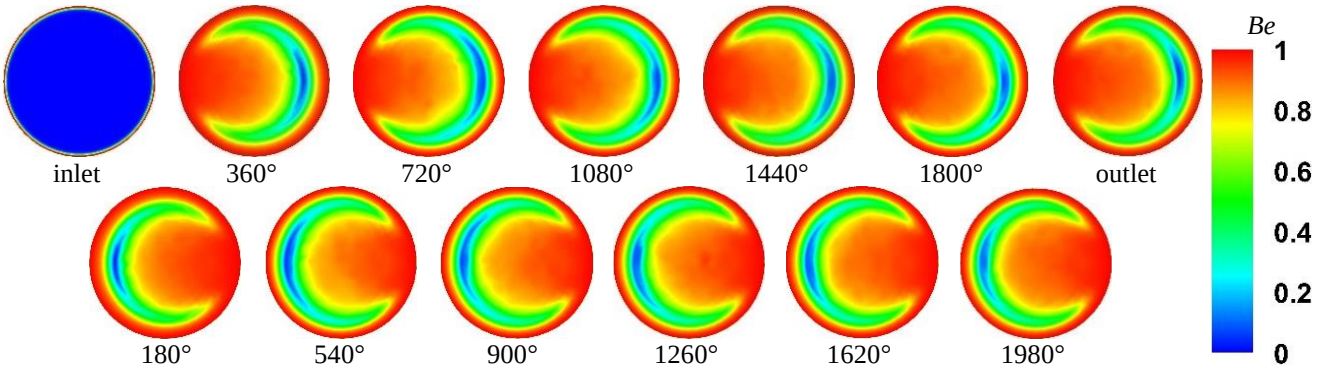

Figure 12. Bejan number contours for different cross sections of the tube

Figure 13 summarizes the order of magnitude of the contribution of viscous friction effects and thermal effects in the total generation of entropy. The increase in the wall heat flux involves an increase in the Bejan number.

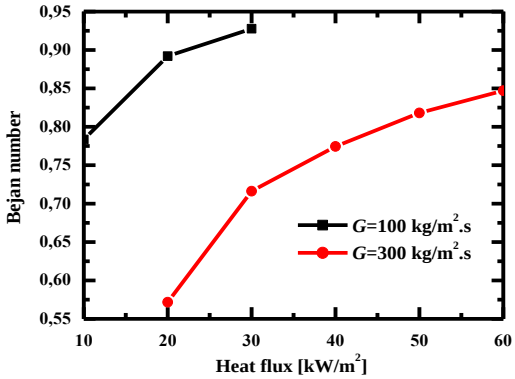

Figure 13. Effect de the wall heat flux on the Bejan number

4. CONCLUSION

In this study, the analysis of the entropy generation of the fully developed turbulent heat transfer flow in a helically coiled tube is numerically studied. The validation of the numerical model is carried out by comparisons with experimental data. The velocity and temperature contours are presented in several transverse stations along the tube. The maximum values of the entropy generation due to local heat transfer are mainly located in the region of the boundary layer, while the maximum values of the entropy generation due to viscous effects are mainly located in a thin layer near the wall and almost uniform in the center of the tube. The Be is greater than 0.5 in all the cases studied.

REFERENCES

1. S. Wang, W. Zhang, J. Xu, 2013, Experimental investigation on flow characteristics of supercritical CO_2 in a helically coiled tube, Applied Mechanics and Materials, **368 (370)**, pp. 631-635
2. F. Li, B. Bai, 2018, Flow and heat transfer of supercritical water in the vertical helically- coiled tube under half-side heating condition, Applied Thermal Engineering, **133**, pp. 512-519
3. W. Bai, S. Zhang, H. Li, X. Xu, 2019, Effects of abnormal gravity on heat transfer of supercritical CO_2 in heated helically coiled tube, Applied Thermal Engineering **159**, pp. 113833
4. X. Liu, X. Xu, C. Liu , J. He, C. Dang, 2019, The effect of geometry parameters on the heat transfer performance of supercritical CO_2 in horizontal helically coiled tube under the cooling condition, International Journal of Refrigeration **106**, pp. 650–661

5. S. Zhang , X. Xu, C. Liu, X. Liu , Z. Ru, C. Dang, 2020, Experimental and numerical comparison of the heat transfer behaviors and buoyancy effects of supercritical CO_2 in various heating tubes, International Journal of Heat and Mass Transfer, **149**, 119074
6. S. Zhang, X. Xu, C. Liu, X. Liu, Y. Zhang, C. Dang, 2019, The heat transfer of supercritical CO_2 in helically coiled tube: Trade-off between curvature and buoyancy effect, Energy **176**, pp. 765-777
7. Z. Zhao, D. Che, Y. Zhang, S. Yao, K. Zhang, Y. Lin, 2015, Numerical investigation on conjugate heat transfer to supercritical CO_2 in membrane helical coiled tube heat exchangers, Numerical Heat Transfer, part A, **1109330**
8. X. Xu, C. Liu, C. Dang, Y. Wu, X. Liu, 2016, Experimental investigation on heat transfer characteristics of supercritical CO_2 cooled in horizontal helically coiled tube, International Journal of Refrigeration, **67**, pp. 190-201
9. X. Xu, Y. Zhang, C. Liu, S. Zhang, C. Dang, 2018, Experimental investigation of heat transfer of supercritical CO_2 cooled in helically coiled tubes based on exergy analysis, International Journal of Refrigeration **89**, pp. 177–185
10. N. T. Rao, A. N. Oumer, G. Devandran, M. M. Noor, 2018, Investigation on Flow and Heat Transfer of Supercritical CO_2 in Helical Coiled Tubes at Various Supercritical Pressures, MATEC Web of Conferences **225**, 01018
11. R.N. Xu, F. Luo, P.X. Jiang, 2015, Experimental research on the turbulent convection heat transfer of supercritical pressure CO_2 in a serpentine vertical mini tube, Int. J. Heat Mass Transf. **91**, pp. 552–561.
12. Z.H. Li, Y.L. Zhai, K.Z. Li, H. Wang, J.F. Lu, 2016, A quantitative study on the interaction between curvature and buoyancy effects in helically coiled heat exchangers of supercritical CO2 Rankine cycles, Energy **116**, pp. 661–676.
13. W. Zhang, S. Wang, C. Li, et al., 2015, Mixed convective heat transfer of CO_2 at supercritical pressures flowing upward through a vertical helically coiled tube, Appl. Therm. Eng. **88**, pp. 61–70.
14. X. Liu, X. Xu, C. Liu, et al., 2017, Numerical study of the effect of buoyancy force and centrifugal force on heat transfer characteristics of supercritical CO_2 in helically coiled tube at various inclination angles, Appl. Therm. Eng. **116**, pp. 500–515.
15. S.J. Zhang, X.X. Xu, C. Liu, Y.D. Zhang, C.B. Dang, 2018, The buoyancy force and flow acceleration effects of supercritical CO_2 on the turbulent heat transfer characteristics in heated vertical helically coiled tube, Int. J. Heat Mass Transf. **125**, pp. 274–289.
16. K.Z. Wang, X.X. Xu, et al., 2017, Experimental and numerical investigation on heat transfer characteristics of supercritical CO_2 in the cooled helically coiled tube, Int. J. Heat Mass Transf. **108**, pp. 1645–1655.
17. J.L. Xu, C.Y. Yang, W. Zhang, D.L. Sun, 2015, Turbulent convective heat transfer of CO2 in a helical tube at near-critical pressure, Int. J. Heat Mass Transfer **80**, pp. 748–758.
18. X.X. Xu, Y.Y. Wu, C. Liu, K.Z. Wang, J. Ye, 2015, Numerical study of cooling heat transfer of supercritical carbon dioxide in a horizontal helically coiled tube, Acta Phys. Sin. **64** (5), pp. 1–7.
19. K.Z. Wang, X.X. Xu, Y.Y. Wu, C. Liu, C.B. Dang, 2015, Numerical investigation on heat transfer of supercritical CO2 in heated helically coiled tubes, J. Supercrit. Fluids **99**, pp. 112–120.
20. A. Bejan, 1982, Entropy Generation through Heat and Fluid Flow, Wiley, New York
21. A. Bejan, 1996, Entropy generation minimization: the new thermodynamics of finite size devices and finite-time processes, J. Appl. Phys. **79**, pp. 1191–1218.
22. K. Safer, A. Ouadha, F. Tabet, 2017, Entropy generation in turbulent syngas counter-flow diffusion flames, International Journal of Hydrogen Energy, **42**, pp. 29532-29544.
23. A. Khait, Noskov, , V. Bianco, 2018, Analysis of the local entropy generation in a double-circuit vortex tube, Applied Thermal Engineering, **130**, pp. 1391–1403
24. F. Kock, H. Herwig, 2004, Local entropy production in turbulent shear flows: a high-Reynolds number model with wall functions, Int. J. Heat Mass Transf. **47**, pp. 2205–2215.
25. F. Kock, H. Herwig, 2005, Entropy production calculation for turbulent shear flows and their implementation in CFD codes, Int. J. Heat Fluid Flow **26**, pp. 672–680.
26. R.Z. Gong, N.M. Qi, H.J. Wang, A.L. Chen, D.Q. Qin, 2017, Entropy Production Analysis for S-Characteristics of a Pump Turbine, Journal of Applied Fluid Mechanics, **10**(6), pp. 1657–1668
27. Paoletti S, Rispoli F, Sciubba E., 1989, Calculation of exergetic losses in compact heat exchanger passages. ASME AES, **10**, pp. 21–9.
28. F.R. Menter, 1994, Two-equation Eddy-viscosity models for engineering applications, AIAA J., **32**, pp. 1598-1605.